Supplementary Information for

Complex rupture process on the conjugate fault system of the 2014 Mw 6.2 Thailand earthquake

Tira Tadapansawut[1,*], Yuji Yagi[2,], Ryo Okuwaki[2,3,4], Shinji Yamashita[5], & Kousuke Shimizu[5]**

[1] Graduate School of Life and Environmental Sciences, University of Tsukuba, Tsukuba, Ibaraki 305-8572, Japan.

[2] Faculty of Life and Environmental Sciences, University of Tsukuba, Tsukuba, Ibaraki 305-8572, Japan

[3] Mountain Science Center, University of Tsukuba, Tsukuba, Ibaraki 305-8572, Japan.

[4] COMET, School of Earth and Environment, University of Leeds LS2 9JT, UK.

[5] Graduate School of Science and Technology, University of Tsukuba, Tsukuba, Ibaraki 305-8572, Japan

[*] Corresponding author: Tira Tadapansawut (tira.tadapansawut@gmail.com)

[**] Second corresponding author: Yuji Yagi (yagi-y@geol.tsukuba.ac.jp)

Contents of this file

Text S1. Uncertainty and sensitivity analyses of the potency density tensor inversion

The sensitivity analysis of the minimum percentage of the relative weight smoothness constraint shows that when it is set to 5%, 10% and 20%, the solutions do not visibly differ (Fig. S2). The total moment tensor solution and the moment-rate function show consistent solutions. The locations of the largest potency density tensor also show similar locations in the middle of the EWTA among the solutions. The strike orientation of the potency density is also robustly resolved in the middle of the NSTA and EWTA.

The sensitivity of the near-source structure model is tested against the CRUST1.0 model (Laske et al., 2013) (Table S2) and the regional structural model by Wongwai et al. (2013) (Table S1) (Fig. S4). The results show that the strike orientation of the potency density tensor is robustly resolved in the middle of both the NSTA and the EWTA even the different velocity models have been applied. However, the amplitudes of the moment-rate functions are slightly different, probably due to the different velocity and thickness of the first layer (Tables S1 and S2).

We test the total rupture duration assumption at 6, 8, 10, and 12 s (Fig. S6). The rupture process during 0–5 s is robustly resolved among the solutions, but we found that the later period, e.g., during 6–12 s is affected by the assumption of total duration. Given this possible uncertainty in the later period after 5 s, we here focus our result and discussion on the robust rupture process during 0–5 s in the main text.

The sensitivity of the maximum velocity assumption has been tested at 3.2 km/s, 3.6 km/s (this study), and 4.0 km/s (Fig. S7). The analysis shows that the maximum rupture velocity assumption of the 2014 Thailand earthquake does not affect the solution. Thus, we choose to use the value of 3.6 km/s which is similar to the structural velocity model at 5 km depth of Wongwai et al. (2013) for our study.

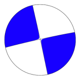 Mainshock	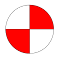 M1	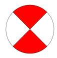 M2	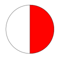 M3	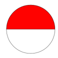 M4	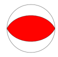 M5
Normalized moment tensor solution (GCMT, 2014)	0.976	1.000	0.207	0.079	0.015
Percent of the relative smoothness constraint (W_q)	5.13%	5.00%	24.19%	63.08%	100.00%

Figure S1. The summary of the relative weight smoothness constraint for each basis moment tensor component from M1 to M5 (Kikuchi & Kanamori, 1991). The blue beachball represents the GCMT solution (GCMT, 2014).

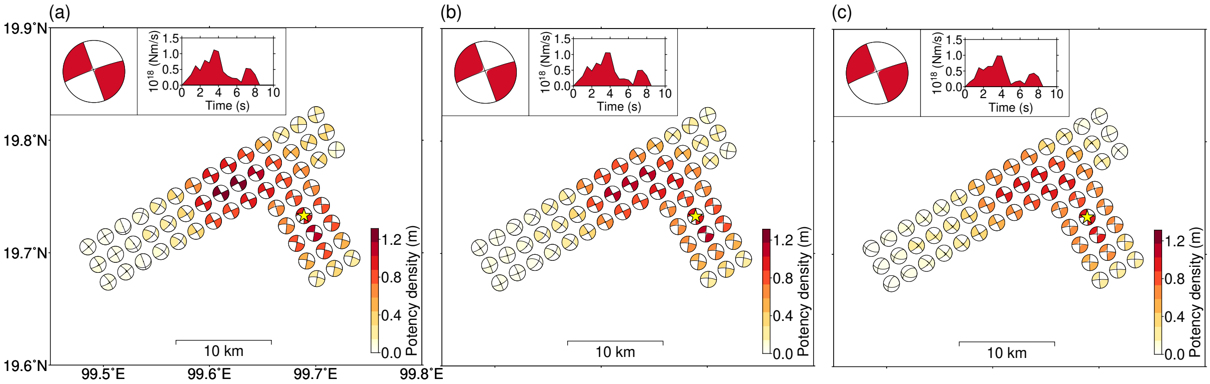

Figure S2. The comparison of the results adopting the different weight smoothness constraints of (a) 5%, (b) 10% and (c) 20% of the maximum relative standard deviation. The map shows the focal mechanism distribution of the potency density tensor of each sub-fault. The color shows the amount of potency density. The star denotes the epicenter. The insets show the total moment tensor solution and the moment-rate function.

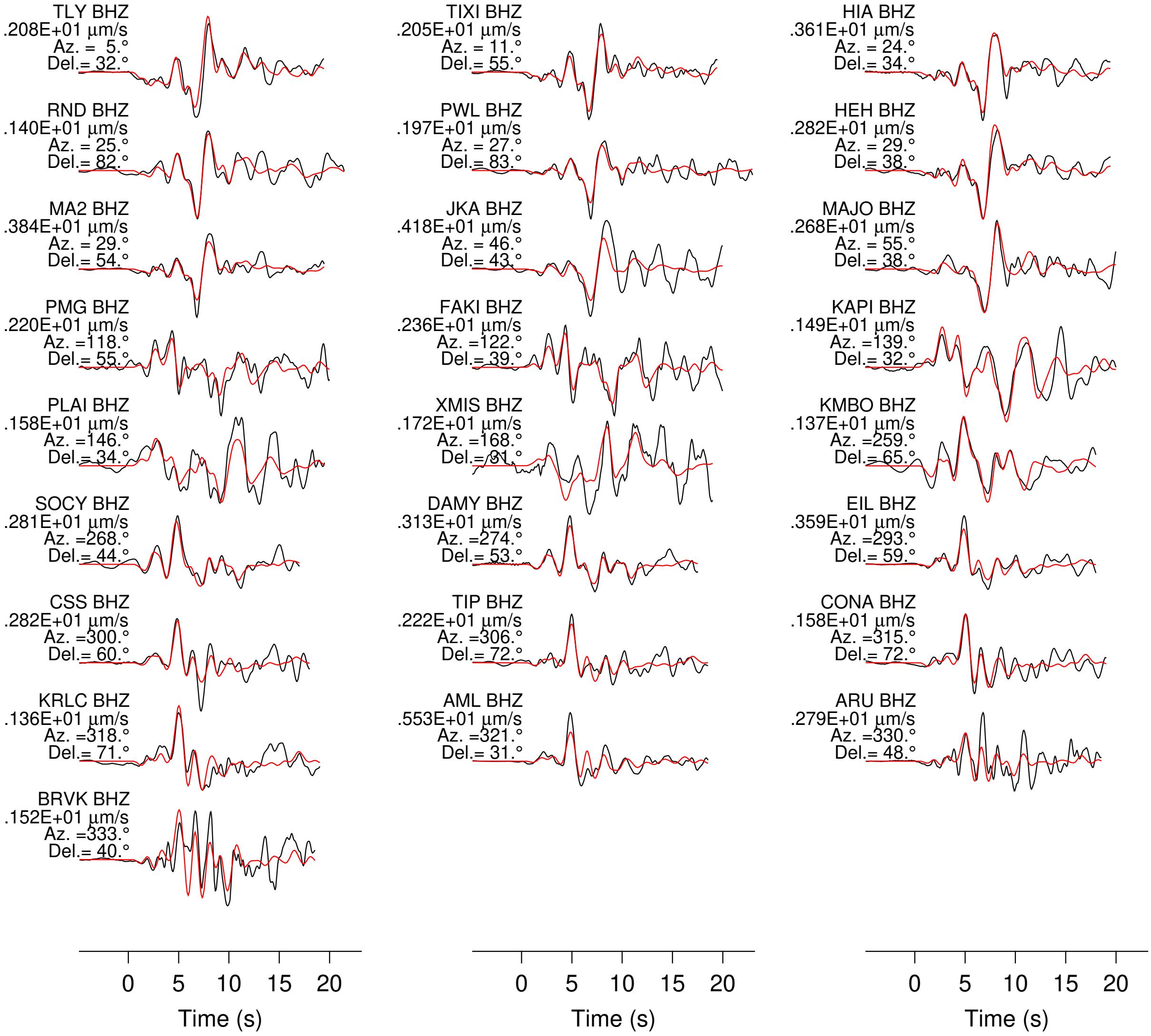

Figure S3. The waveform fitting between the observed waveform (black) and the synthetic (red) waveform of the 2014 Thailand earthquake. Station code, maximum amplitude, azimuth (Az.), and epicentral distance (Del.) are shown on the top-left of each panel.

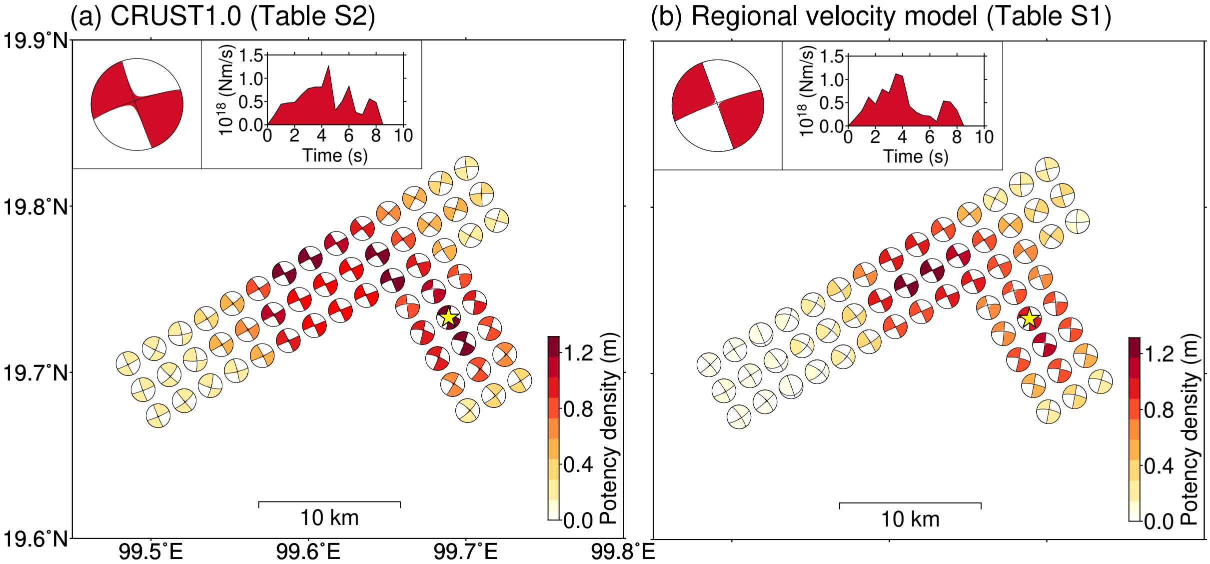

Figure S4. The summary of the sensitivity test of the near-source structure models using the (a) CRUST1.0 model (Laske et al., 2013) (Table S2) and the (b) regional velocity model (Wongwai et al., 2013) (Table S1). The map shows the focal mechanism distribution of the potency density tensor at each sub-fault. The star denotes the epicenter. The insets show the total moment tensor solution and the moment-rate function.

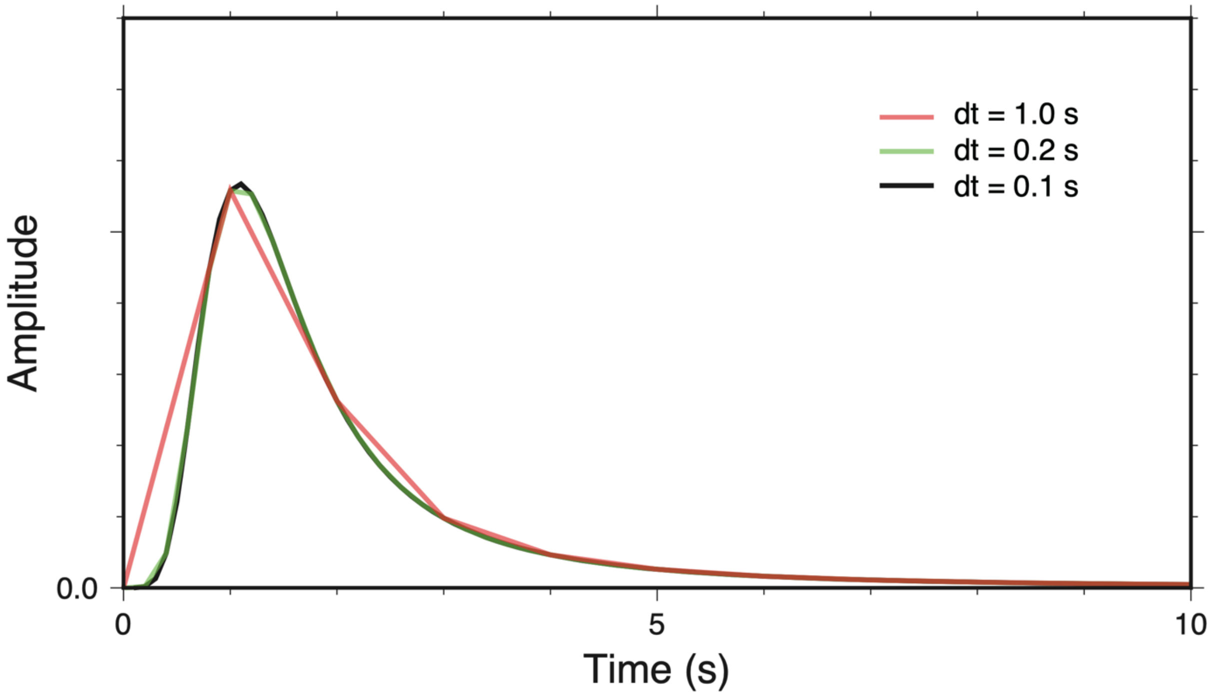

Figure S5. An impulse response function of the effect of inelastic attenuation of the Earth. The program of Kikuchi and Kanamori (1991) is used for the calculation, and the attenuation time constant t* is set to 1.0 s. The black, green, and red lines represent the sampling interval at 0.1 s, 0.2 s, and 1.0 s, respectively.

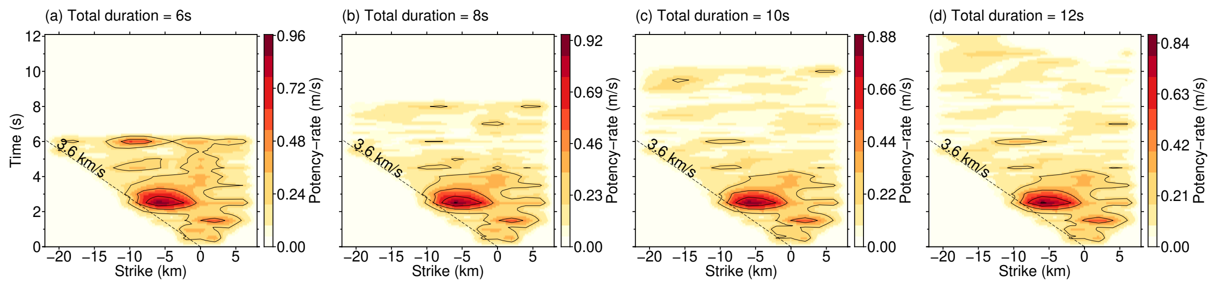

Figure S6. The summary of the sensitivity test of the total rupture duration assumption at (a) 6 s, (b) 8 s, (c) 10 s, and (d) 12 s. The panel shows the spatiotemporal distribution of the potency-rate density projected along the strike 60° of the assumed model plane. The dashed line denotes the maximum rupture-front velocity adopted in our inversion.

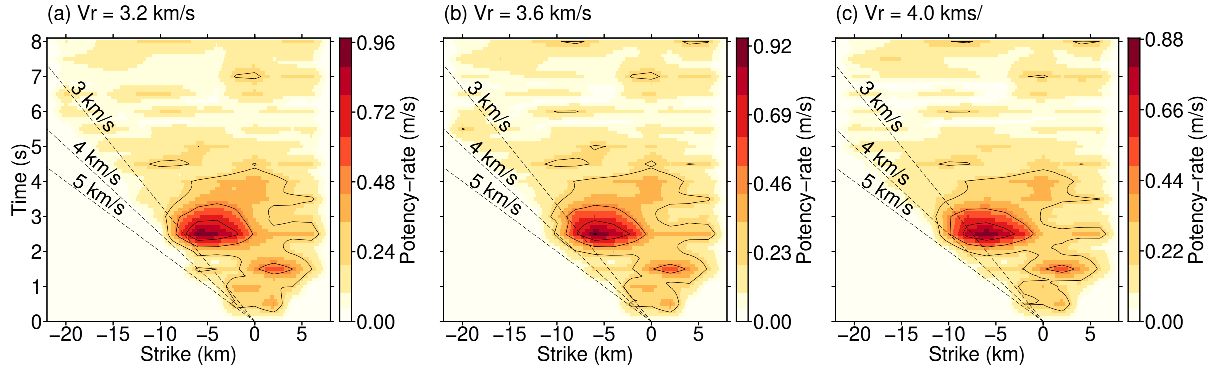

Figure S7. The summary of the sensitivity test of the maximum rupture velocity assumption at (a) 3.2 km/s, (b) 3.6 km/s, and (c) 4.0 km/s. The panel shows the spatiotemporal distribution of the potency-rate density projected along the strike 60° of the assumed model plane. The dashed line denotes the reference rupture-front velocity.

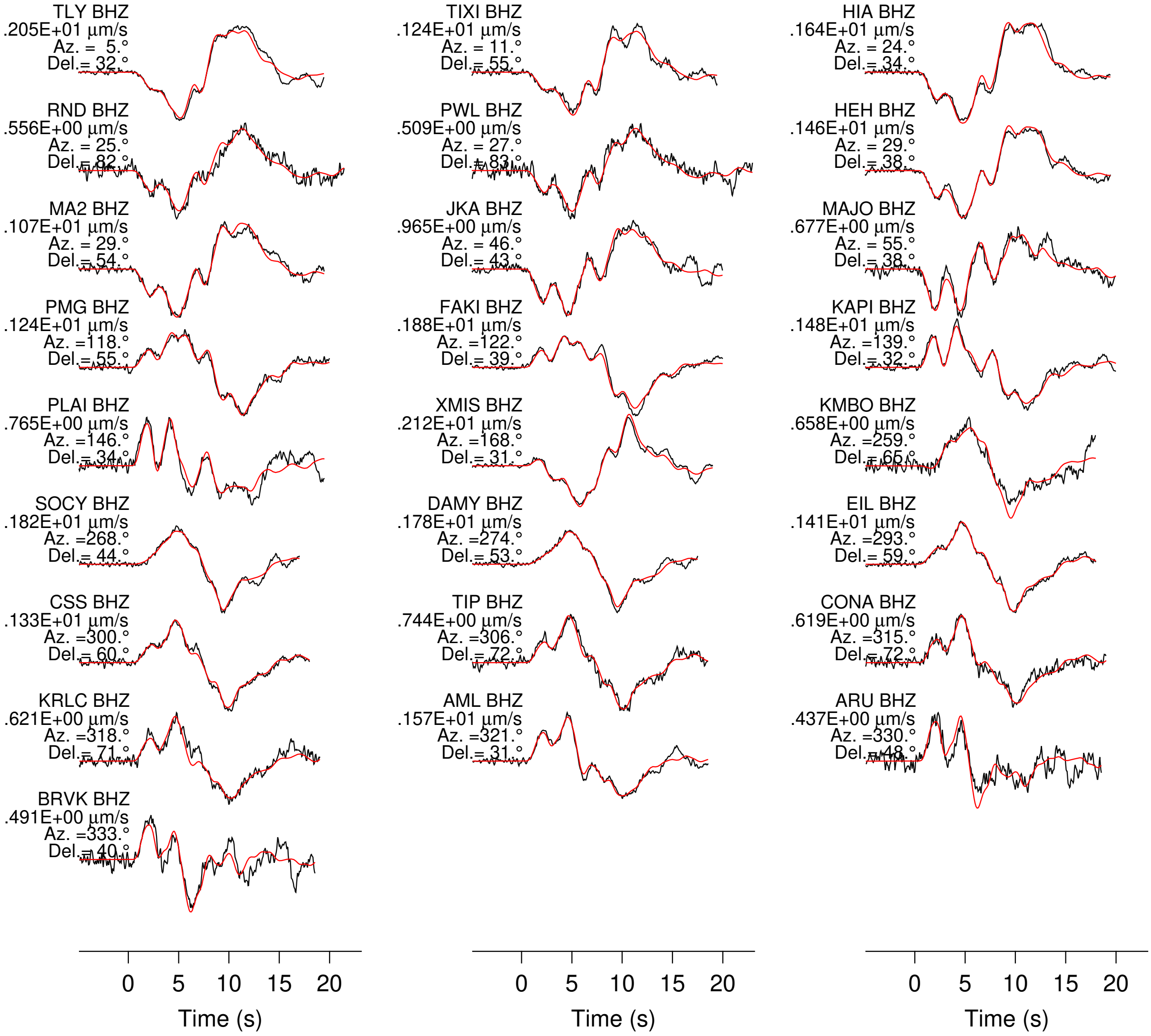

Figure S8. The waveform fitting between the input (black) and output (red) waveforms from the numerical test (Figs. 4 and 5). Station code, maximum amplitude, azimuth (Az.), and epicentral distance (Del.) are shown on the top-left of each panel.

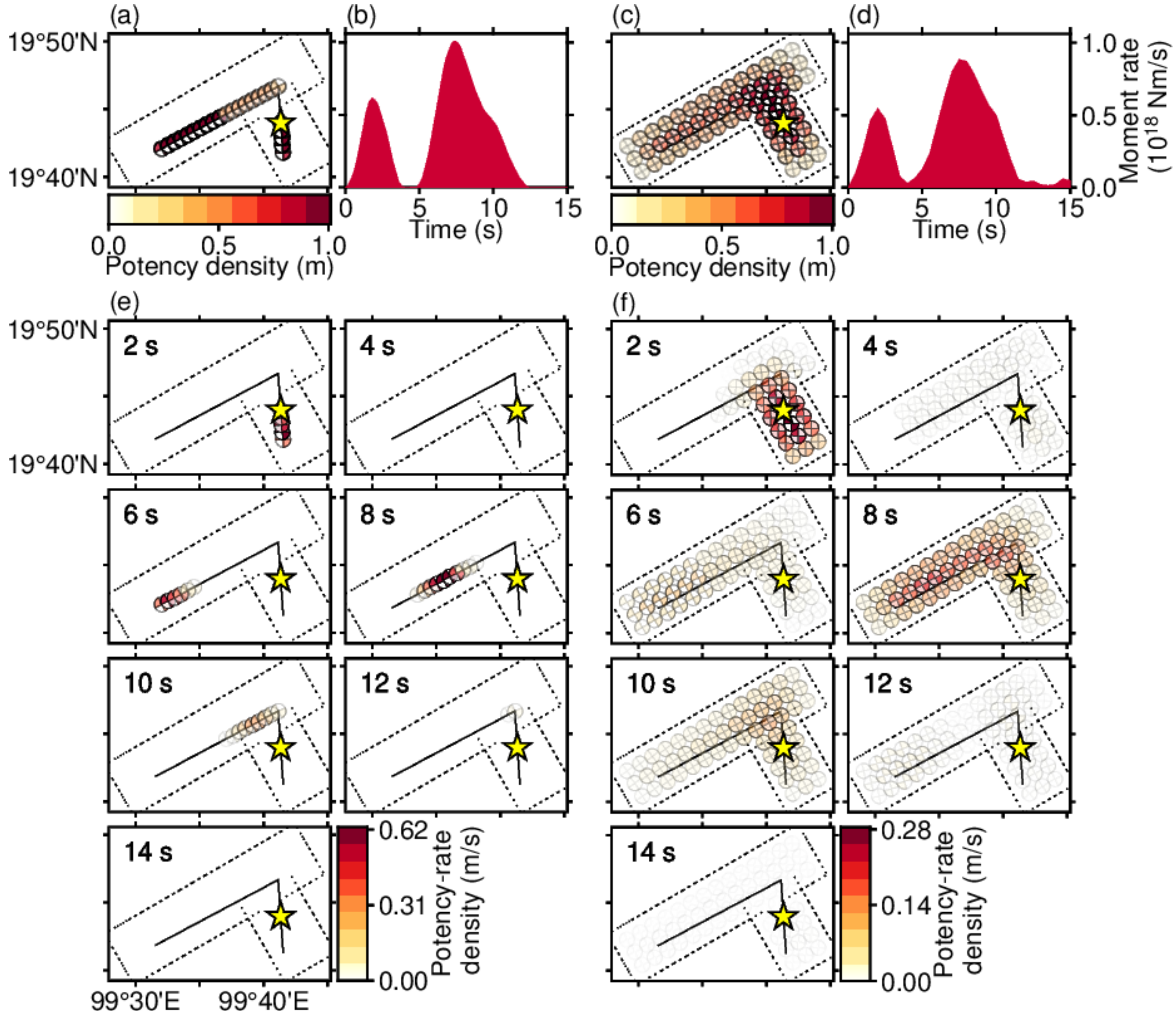

Figure S9. Summary of the numerical test of the input of rupture propagating toward NE along Fault 2. (a) The map-view of the input potency density tensors. (b) The input moment-rate function. (e) The spatiotemporal distribution of the input potency-rate density tensors. Only the non-zero potency-rate density tensor located at the same depth as the hypocenter is shown. (c–f) Similar as the panels (a–c) but for the output solution. The star indicates the initial rupture point. The solid lines show the input faults. The dotted line denotes the assumed horizontal model plane.

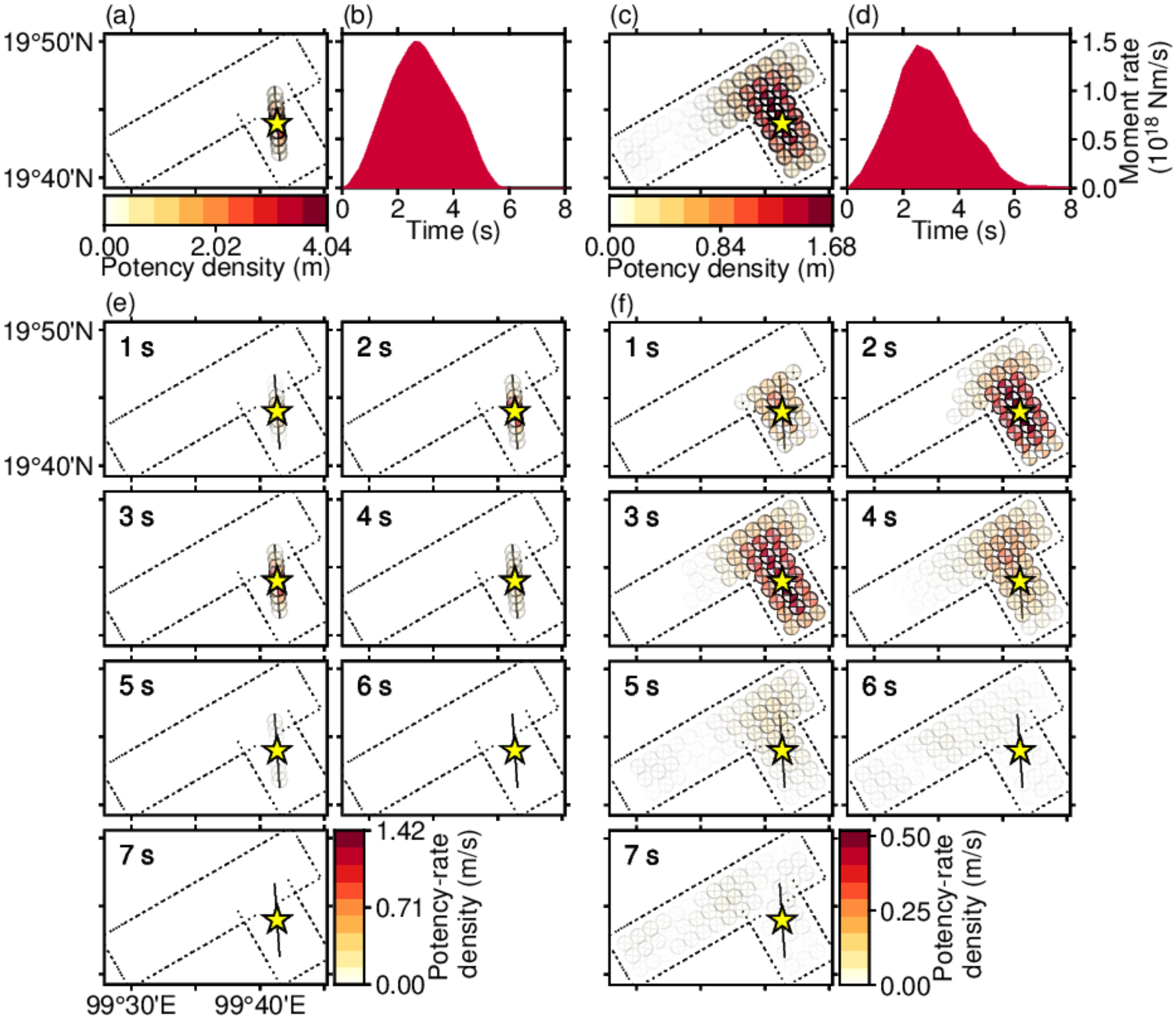

Figure S10. Summary of the numerical test of one input rupture fault of the Fault 1. (a) The map-view of the input potency density tensors. (b) The input moment-rate function. (e) The spatiotemporal distribution of the input potency-rate density tensors. Only the non-zero potency-rate density tensor located at the same depth as the hypocenter is shown. (c–f) Similar as the panels (a–c) but for the output solution. The star indicates the initial rupture point. The solid lines show the input faults. The dotted line denotes the assumed horizontal model plane.

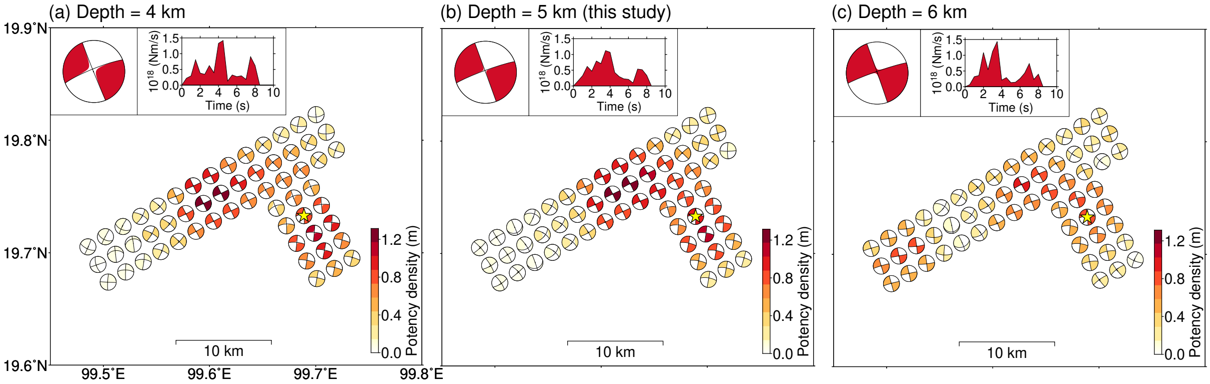

Figure S11. The summary of the sensitivity test of the different model plane depth at (a) 4 km, (b) 5 km, and (c) 6 km. The map shows the focal mechanism distribution of the potency density tensor at each sub-fault. The color shows the amount of potency density. The star denotes the epicenter. The insets show the total moment tensor solution and the moment-rate function.

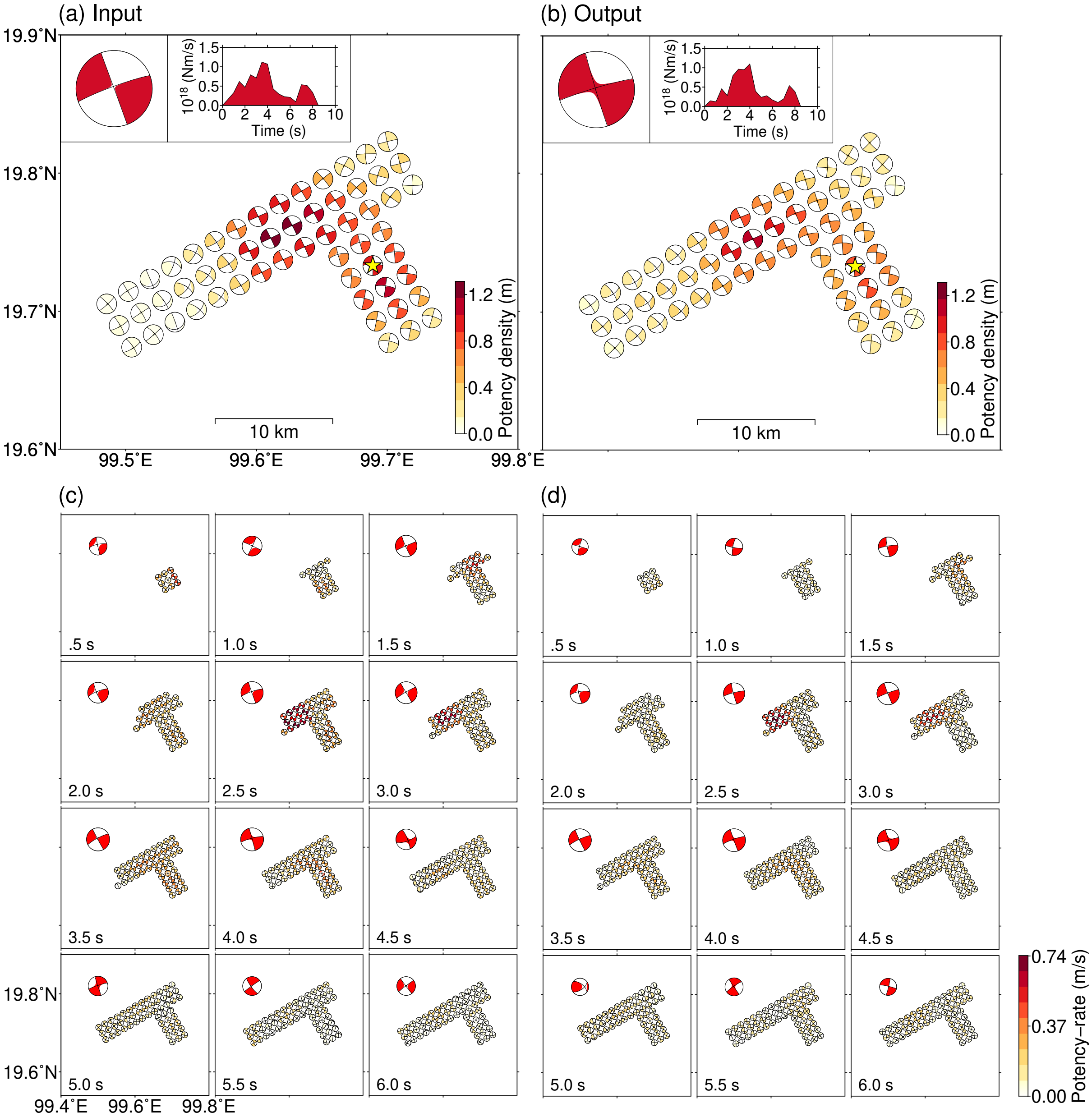

Figure S12. The summary of the reproduction test. The panels (a) and (c) show the input and (b) and (d) show the output. The upper map shows the focal mechanism distribution of the potency density tensor at each sub-fault. The color shows the amount of potency density. The star denotes the epicenter. The insets show the total moment tensor solution and the moment-rate function. The lower panels show snapshots of the focal mechanism distribution of the potency-rate density tensor at each sub-fault. The red beach ball shows the total moment tensor solution within the time window. The color shows the potency-rate density.

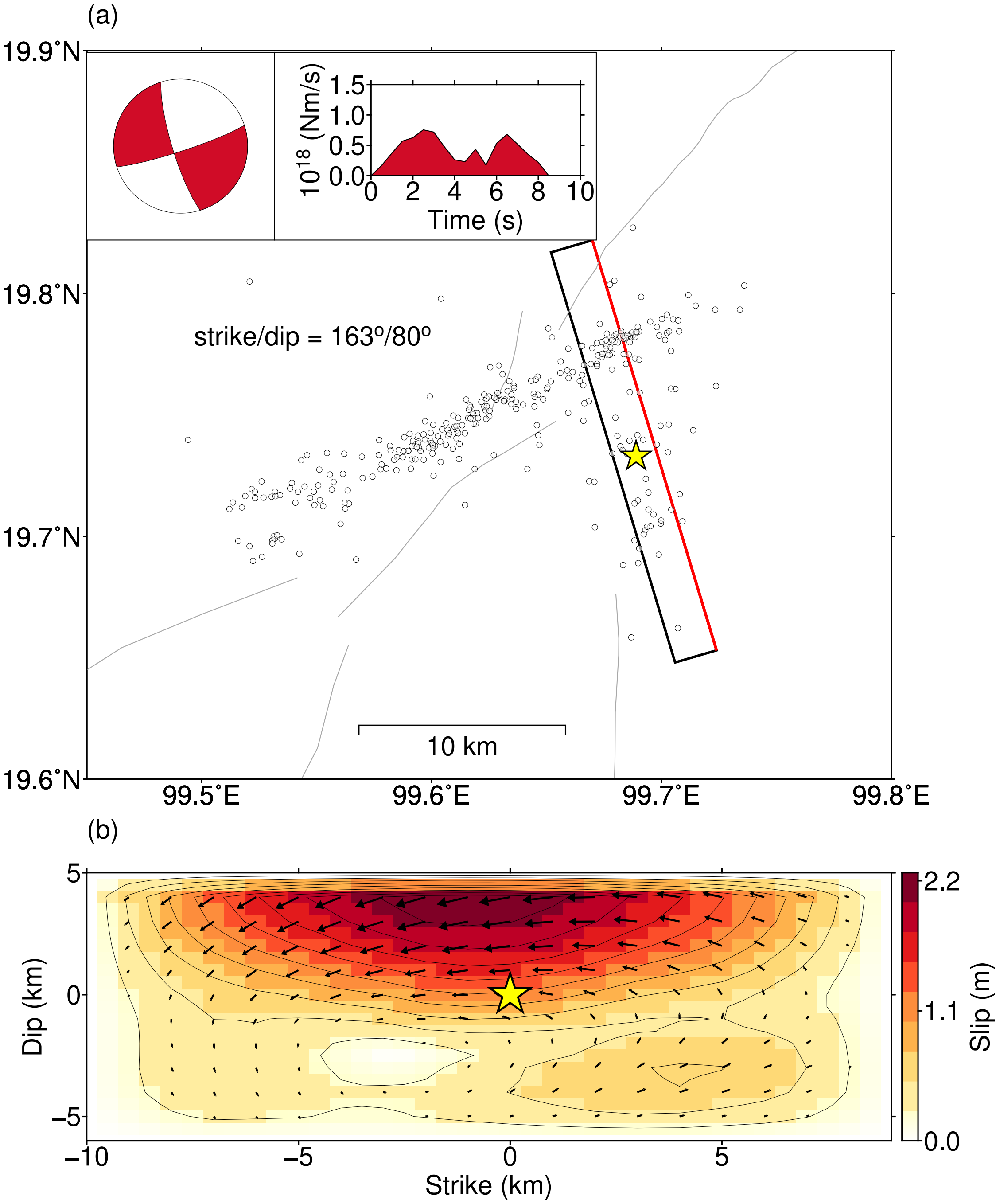

Figure S13. The summary of a single vertical fault plane analysis. (a) The assumed model plane along N-S. The sub-fault has a dimension of 1 × 1 km^2 along strike and dip. The total length is 19 km and width is 11 km. The hypocentral depth is set at 5.0 km. The moment-rate function for each sub-fault is represented as a linear B-spline function with a 0.5 s interval. The total rupture duration is set at 8.0 s. The maximum rupture velocity is set at 3.6 km/s. The red line is the upper bound of the mode plane. The star denotes the hypocenter. The insets show the total moment tensor solution and the moment-rate function. The panel (b) shows the slip distribution of the assumed source model. The arrow denotes the basis slip vector.

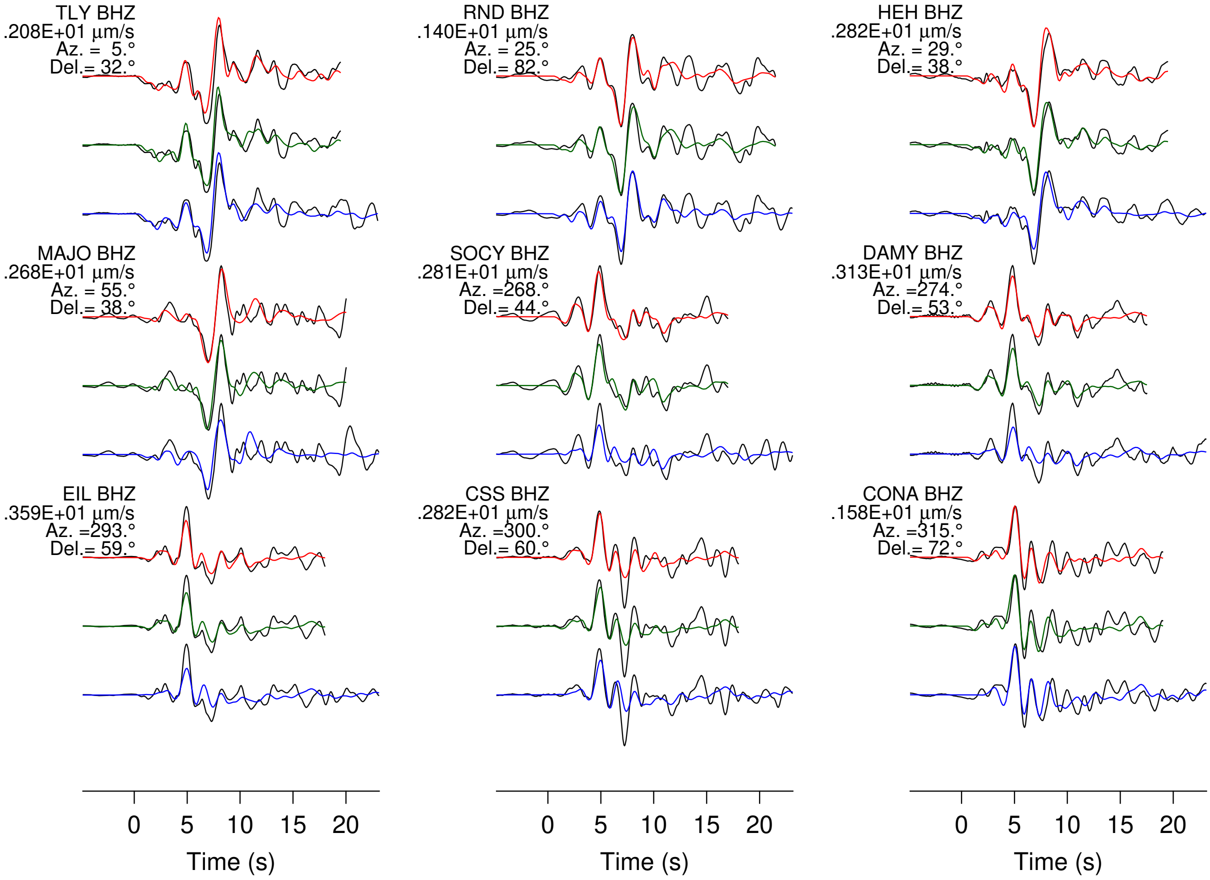

Figure S14. The waveform fit between the observed waveform (black) and the synthetic waveform of our study (red), an assumed horizontal plane covering only on the N-S analysis in Fig. S15 (green), and a single vertical mode plane analysis in Fig. S13 (blue). Station code, maximum amplitude, azimuth (Az.), and epicentral distance (Del.) are shown on the top-left of each panel. The variance reduction (Shimizu et al., 2021) of the waveform fit exhibits at 73%, 66%, and 54% for our study, a horizontal plane covering only on N-S, and a vertical model plane, respectively.

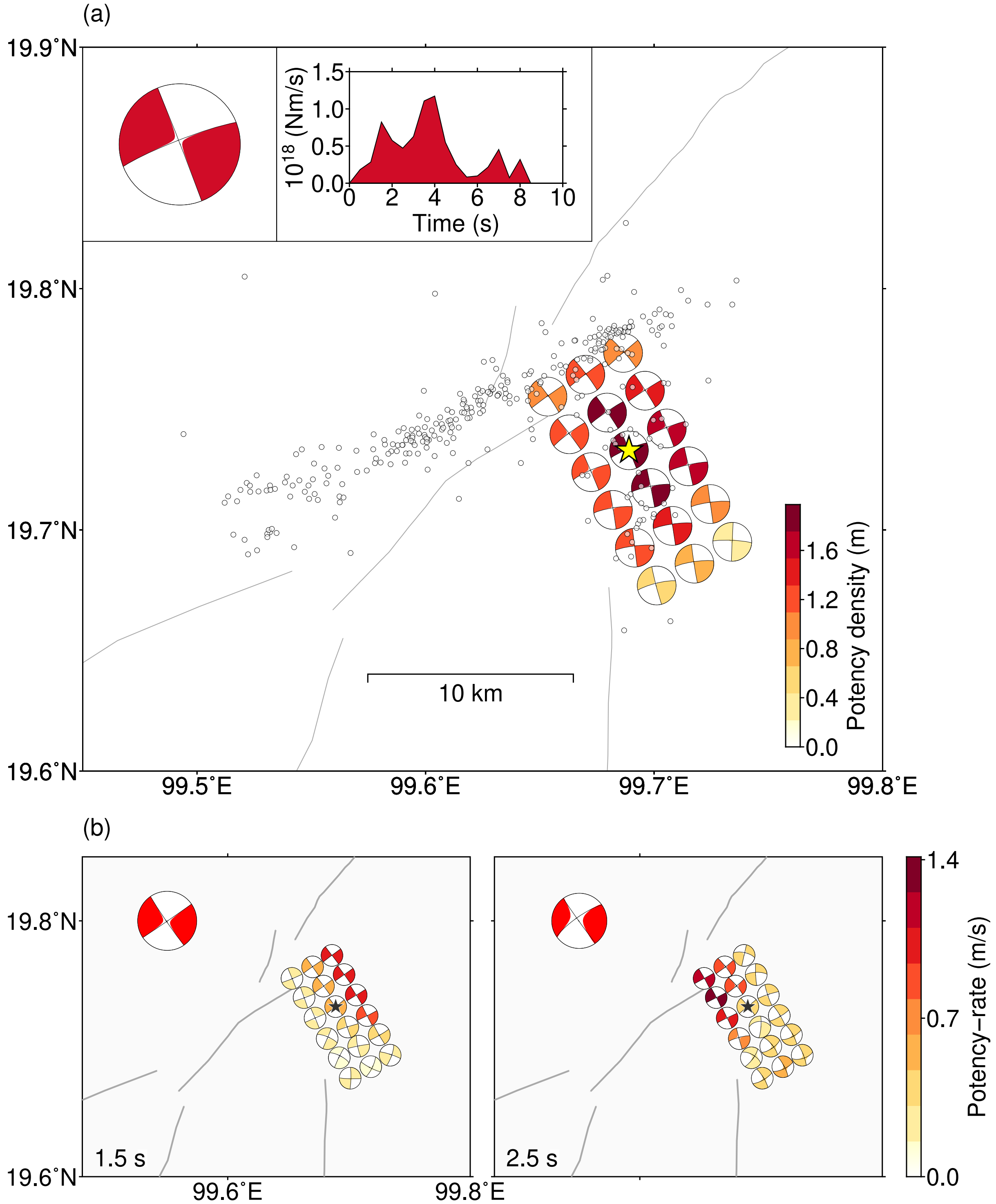

Figure S15. The summary of the analysis assuming a horizontal model plane covering only the N-S segment. The panels (a) show the focal mechanism distribution of the potency density tensor. The color shows the amount of potency density. The star denotes the epicenter. The insets show the total moment tensor solution and the moment-rate function. The panels (b) show the snapshots of the focal mechanism distribution of the potency-rate density tensor. The red beach ball shows the total moment tensor solution within the corresponding time window. The color shows the potency-rate density.

Table S1. Velocity structure (Wongwai et al., 2013) used for calculating Green's function.

V_P (km/s)	V_S (km/s)	Density (10^3 kg/m^3)	Thickness (km)
6.23	3.60	2.80	6.00
6.62	3.83	2.91	6.00
6.78	3.92	2.93	6.00
7.46	4.31	3.13	16.00
8.52	4.92	3.50	0.00

Table S2. Velocity structure used for calculating Green's function made from CRUST1.0 model (Laske et al., 2013).

V_P (km/s)	V_S (km/s)	Density (10^3 kg/m^3)	Thickness (km)
2.50	1.07	2.11	0.67
6.10	3.55	2.74	15.61
6.30	3.65	2.78	30.04
7.00	3.99	2.95	36.33
8.15	4.52	3.36	0.00

References

GCMT (2014) *Moment Tensor for* M_W *6.2 (GCMT) THAILAND*. Retrieved from https://ds.iris.edu/spud/momenttensor/9687293

Kikuchi M, Kanamori H (1991) Inversion of Complex Body Waves-III. *BSSA*, *81*(6), 2335–2350. https://doi.org/10.1785/BSSA0810062335

Laske G, Masters G, Ma Z, Pasyanos M (2013) Update on CRUST1.0–A 1-degree Global Model of Earth's Crust, *Geophys. Res. Abs. 15,* EGU2013–2658. Retrieved from http://igppweb.ucsd.edu/~gabi/rem.html

Shimizu K, Yagi Y, Okuwaki R, Fukahata Y (2021) Construction of fault geometry by finite-fault inversion of teleseismic data. *Geophys J Int*, *224*(2), 1003–1014. https://doi.org/10.1093/gji/ggaa501

Wongwai W, Pananont P, Pornsopin P (2013) Teleseismic Receiver Functions Study of the Crustal Thickness Underneath Thailand. *AGU, Fall Meeting 2013, Abstract Id. S33F-03*. Retrieved from http://adsabs.harvard.edu/abs/2013AGUFM.S33F..03W